Heterogeneous Catalysis

DOI: 10.1002/ange.201101821

Effect of Composition on the Catalytic Properties of Mixed-Ligand-Coated Gold Nanoparticles**

*Anirban Ghosh, Soubir Basak, Benjamin H. Wunsch, Rajiv Kumar, and Francesco Stellacci**

Ligand-coated nanoparticles (NPs) are hybrid materials with novel properties.[1,2] Monolayer-protected gold NPs are emerging as attractive candidates for catalysis,[3,4] in particular as artificial enzymes (nanozymes).[5,6] There are many reasons for their success ranging from the ease of forming dense monolayers of complex catalytic molecules on their ligand shells to their facile separation from the reaction products by precipitation. Herein, we present a study on the effect of composition on the catalytic efficiency of NPs with mixed-monolayer ligand shells. We show that by using simple catalytically inactive molecules it is possible to enhance the catalytic efficiency of NPs.

Recently, we discovered that when two dislike thiolated ligands are co-assembled on the ligand shell of gold NPs, the separation of the two ligands generates stripelike domains that are only a few molecules thick.[7–10] This phenomenon is observed because of a balance between the enthalpy of phase separation and the conformational entropy that longer (or bulkier) ligands gain when surrounded by shorter ones.[11,12] The difference in the chain length of the two ligands renders the stripelike domains molecular grooves with the shorter ligands being embedded in the surface; the bigger the difference in length the more defined the stripes are supposed to be.[11,12] As the ligand ratio changes the morphology of the ligand shell changes; this in turn generates structure-dependent variations in the solubility and interfacial energy of the particles.[13,14] Herein, we study the effect of the composition (and hence the morphology) of the ligand shell on the catalytic activity.

We explore sulfonic-acid-functionalized gold NPs as acid catalysts. For our experiments, 3-mercapto-1-propanesulfonic acid (MPSA) was chosen as the precursor for the sulfonic acid ligands, which are the shorter ligands. The longer ligands are represented by two different types of nonpolar alkanethiols: 1) linear alkanethiols, namely, butanethiol (BT), hexanethiol (HT), octanethiol (OT), decanethiol (DT), and dodecanethiol (DDT) and 2) phenyl-group-terminated alkanethiols, namely, 6-phenylhexanethiol (6-Ph-HT), 8-phenyloctanethiol (8-Ph-OT), and 10-phenyldecanethiol (10-Ph-DT). The choice of MPSA was made because of two reasons. First, we focused on a commercially available inexpensive molecule; second, we found that most of the structure-driven effects take place when the active molecule is inside the supramolecular grooves, and hence the catalytically active ligand needed to be a short molecule.[13,14] Furthermore we chose to test aryl-terminated longer ligands to improve the interaction of the "groove" walls with the reactants. The ligands and the target nanoparticle size were chosen such that the probability of formation of stripelike domains is maximized.[13–16]

The syntheses of phenyl-terminated alkanethiol ligands with alkyl chain lengths 6—10 methylene units long were performed in a two-step process, as depicted in Scheme 1. A

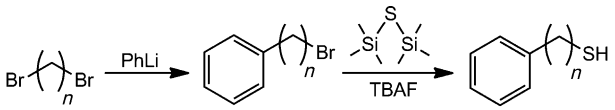

n = 6, 8, 10

Scheme 1. Two-step synthesis of phenyl-terminated alkanethiol ligands.

dibromo alkane of desired alkyl chain length was treated with phenyl lithium under inert atmosphere to form a bromophenyl alkane. The bromide group of the bromophenyl alkane was substituted by a thiol group by treatment with hexamethyldisilathane (HMDT) in the presence of tetrabutylammonium fluoride (TBAF).

To perform comparative studies we tried to synthesize relatively monodisperse NPs. We followed the method introduced by Stucky and co-workers, which involves the *tert*-butylamine borane complex as reducing agent.[17] We observed that this method does not work well with mixed ligand systems, especially, when one or both of the ligands are polar or charged. Therefore, we replaced the usual benzene and chloroform solvent with *N*,*N*-dimethylformamide (DMF), which dissolves sulfonate and alkanethiol ligands simultaneously.

The esterification of carboxylic acids is a fundamental organic transformation. The conversion in esterification

[*] Dr. A. Ghosh, Dr. B. H. Wunsch, Prof. F. Stellacci
Department of Materials Science and Engineering
Massachusetts Institute of Technology
77 Massachusetts Avenue, Cambridge, MA 02139 (USA)
Prof. F. Stellacci
Institute of Materials
École Polytechnique Fédérale de Lausanne
Lausanne, 1015 (Switzerland)
E-mail: francesco.stellacci@epfl.ch
Dr. S. Basak
Department of Chemical Engineering
Massachusetts Institute of Technology (USA)
Dr. R. Kumar
Advanced Materials and Green Chemistry Division
Tata Chemicals Limited, Innovation Centre (India)

[**] Financial support from Tata Chemicals Ltd. is gratefully acknowledged. This work made use of the facilities at the Center for Materials Science and Engineering, MIT and Department of Chemistry Instrumentation Facility, MIT.

Supporting information for this article is available on the WWW under http://dx.doi.org/10.1002/anie.201101821.

reactions is limited by slow reaction rates and by the reversibility of the reactions. Acid catalysts are widely employed in liquid-phase esterification to enhance the reaction rate. The use of homogeneous catalysts such as sulfuric acid and *p*-toluenesulfonic acid suffers from the problems of side reactions, corrosion of the equipment, environmentally hazardous acid waste, and difficulty in separation of the catalyst from the reaction mixture.[18] Use of MPSA, or other equivalent sulfonic-acid-terminated molecules as homogeneous catalysts will also pose similar problems. However, sulfonic acid ω-functionalized gold NPs (both the striped and homoligand particles)[15] are noncorrosive, and can be easily recovered by centrifugation or filtration and reused. We note that the Au NPs tested here are insoluble in the reaction mixture before and after the reaction, and can be separated easily by centrifugation. The recycled catalyst also has similar activity compared to the parent one (results not shown). Therefore, the sulfonic-acid-protected Au NPs act truly as heterogeneous catalysts. We chose acetylation of benzyl alcohol (BzOH) as a test reaction, because the product benzyl acetate (BzAc) is a widely used plasticizer, solvent, odorant, flavor chemical, and also a precursor for a range of pharmaceuticals, agrochemicals, and other fine chemicals.[19] Currently, zeolites with a large number of acidic sites such as Faujasite (USY) are used to produce BzAc through a heterogeneous catalytic process.[20] Here, we show that sulfonate Au NPs—mainly when coated with binary mixtures of ligands—relative to the zeolite catalyze the reaction with a faster reaction rate, and a desired product selectivity close to 100% (as compared to around 80% for the zeolite catalyst).

We chose the esterification of carboxylic acids through acid catalysis because its mechanism excludes cooperative interactions between the acid groups. Scrimin and co-workers have shown that NPs can be ideal for catalysis when cooperative effects occur between catalysts constrained on the surface of nanoparticles.[21] Here, we study morphology effects that go beyond the clustering of catalytic ligands to complement the studies by Scrimin and co-workers.

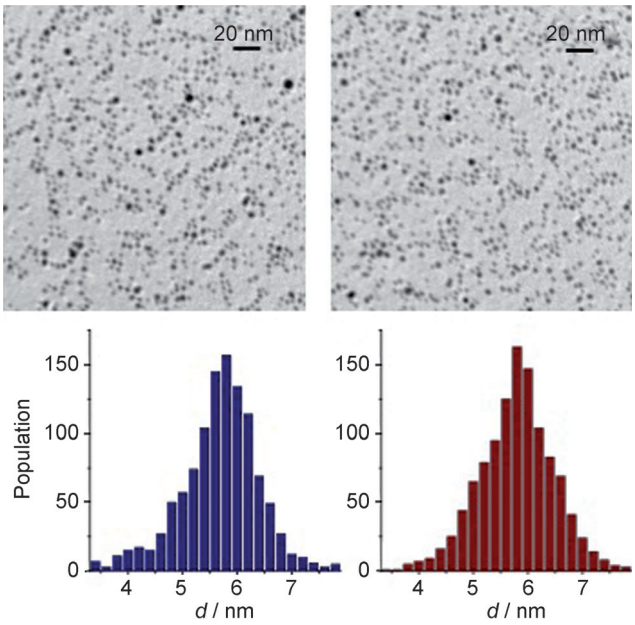

Figure 1. TEM images of Au NPs functionalized with a mixture of MPSA and OT at 2:1 molar ratio (top left), and pure MPSA (top right), with their corresponding size distribution.

The average size distribution for the NPs was calculated from TEM images (Figure 1, summary in Table 1). The chosen synthetic procedure delivers NPs (5–6 nm) of similar core sizes with a relatively low standard deviation (around 20%). The particle sizes are within the size limits for which stripelike domains have been observed.[16] Figure 2 shows representative Au 4f and S 2p core-level spectra for an MPSA–Au nanocomposite sample. The S 2p spectrum has two components at binding energies of 162.6 and 168 eV, which can be attributed to two different oxidation states of sulfur (−2 and +5, assigned to the thiolate and sulfonic acid sulfur groups, respectively) present in the sample. The quantification of the S 2p and O 1s spectra of all the samples are summarized in Table 1. The observed weight ratio of S

Table 1: Compositional and catalytic-activity analysis for Au NPs.

Ligand 1	Ligand 2	Ratio	*c*(ligand 1) [mmol]	*c*(ligand 2) [mmol]	Particle size[a] [nm]	S:O (theo)	O 1s[b] [wt%]	S 2p[b] [wt%]	S:O (obs)	SO_3H[c] [mmol g^{-1}]	Conv.[d] [%]	Sel. [%]	TON[e]
MPSA	None	–	2.00	0.00	5.76±1.48	0.67	7.64	3.71	0.48	0.58	80	>99	692
MPSA	OT	5:1	1.67	0.33	5.77±1.57	0.80	5.97	3.60	0.60	0.56	75	>99	671
MPSA	OT	2:1	1.33	0.67	5.88±1.52	1.00	5.03	3.42	0.68	0.53	85	>99	802
MPSA	OT	1:1	1.00	1.00	5.44±1.58	1.33	3.53	3.45	0.98	0.26	11	>99	212
MPSA	OT	1:2	0.67	1.33	5.55±1.49	2.00	3.31	3.56	1.07	0.25	10	>99	198
MPSA	OT	1:5	0.33	1.67	5.39±1.45	4.00	2.11	4.71	2.22	0.28	8	>99	143
MPSA	BT	2:1	1.33	0.67	5.65±1.47	1.00	3.24	2.12	0.65	0.53	32	>99	301
MPSA	HT	2:1	1.33	0.67	5.42±1.55	1.00	3.06	1.91	0.62	0.50	35	>99	349
MPSA	DT	2:1	1.33	0.67	5.35±1.38	1.00	5.30	3.56	0.67	0.55	81	>99	734
MPSA	DDT	2:1	1.33	0.67	5.28±1.36	1.00	5.28	3.41	0.64	0.53	83	>99	784
MPSA	6-Ph-HT	2:1	1.33	0.67	5.76±1.46	1.00	6.07	4.46	0.73	0.67	86	>99	638
MPSA	8-Ph-OT	2:1	1.33	0.67	5.82±1.39	1.00	5.75	3.81	0.66	0.59	87	>99	737
MPSA	10-Ph-DT	2:1	1.33	0.67	5.64±1.51	1.00	5.19	3.63	0.69	0.56	87	>99	775

[a] From analysis of TEM images. [b] From quantification of XPS core-level spectra; for quantification of the S 2p spectra the total amounts were considered. [c] From integration of the S^{5+} component of the S 2p spectra. [d] Reaction conditions: the ratio of benzyl alcohol to acetic acid was 1:1; 2 wt% catalyst; temperature 80°C; reaction time 6 h. [e] The turnover number (TON) is given as (conversion of BzOH × amount of BzOH in mol)/(amount of -SO_3H groups in mol × 100). The TONs are average values from three experiments with a maximum standard deviation of ±10.

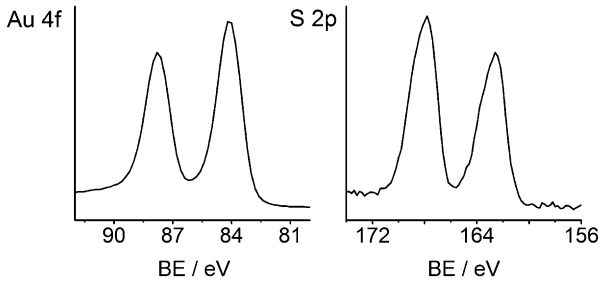

Figure 2. Representative X-ray photoelectron spectra of Au 4f (left side), and S 2p for MPSA–Au NPs (right side). The core-level binding energies (BE) were aligned with respect to the Au $4f_{7/2}$ BE of 84 eV. The S 2p spectrum has two components attributed to S^{5+} and S^{2-} oxidation states, respectively.

and O is lower than the theoretical value, but follows the same increasing trend with decrease in the initial molar ratio of MPSA in the synthetic mixture. The linear correlation between the theoretical and observed S:O ratios is shown in Figure S1 (see the Supporting Information). For different alkanethiols at a fixed molar ratio of MPSA (2:1), the observed S:O weight ratio remains almost constant (around 0.65–0.7). The quantification of the S^{5+} component from the S 2p spectra is necessary to estimate the concentration of catalytically active sites, which in turn was used to calculate the turnover numbers (TONs) of the acetylation reaction given in Table 1. Quantification from XPS might not be fully accurate, because it only shows the surface composition.

Table 1 also summarizes the catalytic activity of all the Au nanoparticle catalysts in terms of conversion of benzyl alcohol, selectivity toward benzyl acetate, and TONs of the acetylation reaction. The respective values for a commercial zeolite USY catalyst are a conversion rate of 51%, selectivity of 76%, and TONs of 84. It should be noted that the conversions represented here are the absolute values observed during the reaction with a fixed amount of NP catalyst (2 wt%).

The TON values represent an authentic comparison of the catalytic efficiency, since the values are normalized with concentration of sulfonic acid groups present on the catalyst surface. All the experiments were performed thrice to check the reproducibility and to estimate the error bars. The MPSA–OT(2:1)–Au, MPSA–DT(2:1)–Au, and MPSA–DDT-(2:1)–Au NPs have much better activity (TON) than MPSA–BT(2:1)–Au and MPSA–HT(2:1)–Au NPs. At present it is hard to draw definitive conclusions on the true reasons for this behavior but we can speculate that a minimum "groove" depth is required to create a favorable effect for the catalysis. This is somewhat also supported by the fact that the MPSA–HT nanoparticles have lower efficiency when compared to the MPSA–6-Ph-HT particles; such a difference disappears when MPSA–OT to MPSA–8-Ph-OT particles are compared. Additionally, as the chain length difference decreases so does the driving force towards the formation of highly defined stripelike domains.[11] Yet, it is not immediately clear how this would affect the catalytic efficiency. In general our complete study on the MPSA–OT system indicates a complex effect of ligand composition and morphology. The highest TON is observed for the 2:1 ratio, followed by the MPSA-rich compositions of 5:1 and the homoligand, all other compositions seem to be poorly active (but still better than the zeolite). These results indicate that the high density of sulfonate groups has a great effect on the catalytic activity but seems to rule out (together with the kinetics data) a simple cooperative effect. At the 2:1 composition at which we expect to see stripelike domains[7,15] we observe the highest activity; all other compositions seem to suggest a dilution effect. If we just compare the TON of the MPSA–OT (ratio of 2:1) nanoparticles to the MPSA homoligand NPs we observe an increase of around 16%. To make sure that this effect was predominantly because of the composition of the ligand shell and structure we performed a similar study on a series of Pt NPs with a similar ligand-shell composition. Interestingly, these series of MPSA–OT-coated Pt NPs revealed a similar trend (see Figures S2, S3, and S4 in the Supporting Information) in the TON with a ligand composition of 2:1 being the most catalytically active. We believe that this result is a strong indication on the role of the ligand shell in the catalytic activity of these particles. We do not have enough data to determine the role of the core material in this catalytic reaction and we believe that its study is beyond the scope of this work. A simple comparison with the Pt particles shows that these particles are more active relative to their Au counterparts. Hence, the core has an effect, yet the trend in the composition of the ligand shell remains mostly identical. Taking into account previous results we suggest that the Au cores have no effect whereas Pt has some effect.[22]

The conversion of benzyl alcohol with increasing time for 1) the homoligand MPSA–Au NPs, 2) MPSA/alkanethiol–Au NPs, 3) MPSA/phenyl-terminated alkanethiol–Au NPs, and 4) the commercial zeolite USY catalyst is shown in Figure 3. The error bars in Figure 3 and in all the subsequent Figures show the standard deviation from the average value of three experiments. The maximum conversion for the nanoparticle catalysts is around 86% at 80°C, whereas for the USY catalyst it is around 51%. Because the reaction is reversible, it is not possible to obtain a conversion of 100% in any case. For the zeolite catalyst, the selectivity toward benzyl acetate was always around 75–80% during the entire course of the reaction. However, for the NP catalysts, the selectivity toward benzyl acetate was always $>99\%$ for all the experiments. Therefore, the selectivity was not shown in Figure 3 or in any of the Figures hereafter.

The MPSA–8-Ph-OT(2:1)–Au NPs have better efficiency in the initial phases of the reaction than the other two nanoparticle catalysts, probably because of the favorable wetting with the reactants. Again, the MPSA–OT(2:1)–Au NPs have slightly better efficiency than the MPSA–Au NPs. The better efficiency of the MPSA/phenyl-terminated alkanethiol—Au NPs at the initial phase of the reaction prompted us to conduct kinetic experiments at a 1:1 molar ratio of benzyl alcohol to acetic acid.

The acetylation of benzyl alcohol is expected to follow second-order kinetics, the reaction is of first order with respect to the concentrations of both benzyl alcohol and acetic acid. For such a reaction, when the initial concentrations of the two reactants are equal, a plot of $1/[BzOH]_t$ versus the reaction time (t) will be linear at conversions smaller than

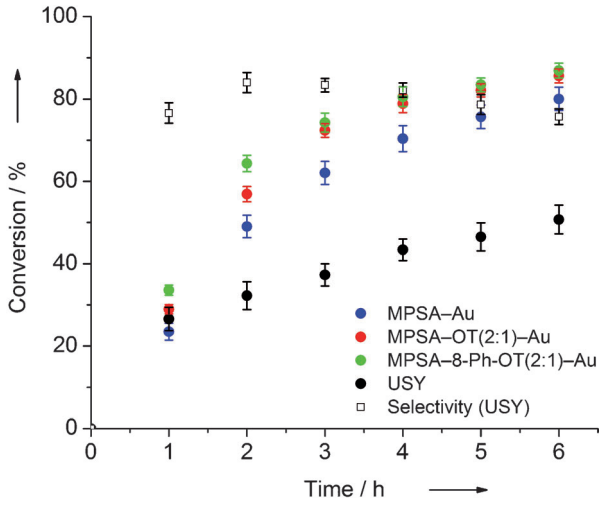

Figure 3. Conversion (solid circles) of benzyl alcohol and selectivity (empty squares) toward benzyl acetate with increasing time (reaction conditions: the ratio of benzyl alcohol to acetic acid was 1:1; 2 wt% Au catalysts, 15 wt% USY; temperature 80 °C).

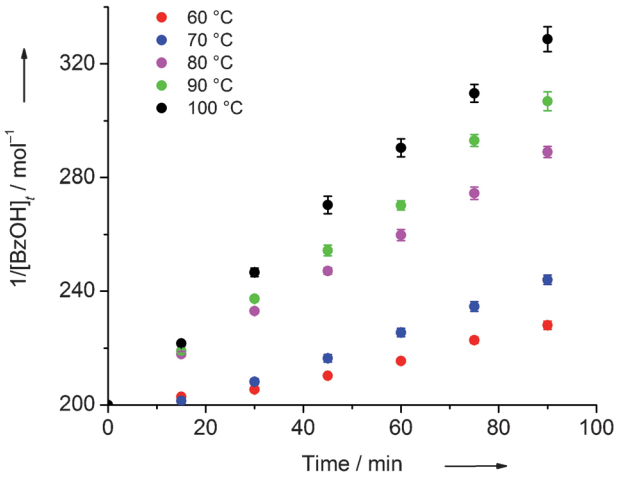

Figure 5. Plot of the reaction rate versus time at different temperatures for MPSA–OT(2:1)–Au nanoparticle as catalyst (reaction conditions: the ratio of benzyl alcohol to acetic acid was 1:1, 2 wt% catalyst). The rate constants were determined from the slope of the respective linear curves.

50%, where $[BzOH]_t$ represents the concentration of BzOH at a given time "t". Figure 4 displays the plot of $1/[BzOH]_t$ versus "t" at 80 °C for three representative catalysts: 1) the homoligand MPSA–Au NPs, 2) the MPSA/alkanethiol–Au NPs, and 3) the MPSA/phenyl-terminated alkanethiol–Au NPs. The reaction rate increases linearly with time. The MPSA–8-Ph-OT(2:1)–Au NPs have a much faster reaction rate than the other two catalysts, which corroborates our previous observation (Figure 3).

Figure 5 shows the plot of $1/[BzOH]_t$ versus "t" for the MPSA–OT(2:1)–Au NPs at different temperatures ranging from 60–100 °C. The reaction rate was low at temperatures of 60–70 °C, and at temperatures higher than 80 °C the reaction rate is considerably enhanced. From the slope of the curves, the rate constants (k) at different temperatures were evaluated. Figure 6 represents the Arrhenius plot of ln k versus $1/T$ for the three catalysts mentioned in Figure 4. Interestingly, the plot is linear for the first three data points, and also for the last three data points. That is, the curve has two different gradients with increasing temperature. There are two possible explanations of this nonlinearity of the Arrhenius plot. The first one could be that there are two different mechanisms operating at different temperatures. However, we have observed that the difference between rate constants at 60 and 70 °C, at 80 and 90 °C, and also at 90 and 100 °C are similar (Figure 5). That is, the reaction rate shows a similar temperature dependence at low and high temperature regimes. Therefore, we believe that two different mechanisms are unlikely. Esterification reactions in the liquid phase follow a standard acid-catalyzed mechanism (see Scheme S1 in the Supporting Information). The alternative explanation is that with increasing temperature, and specifically after a certain

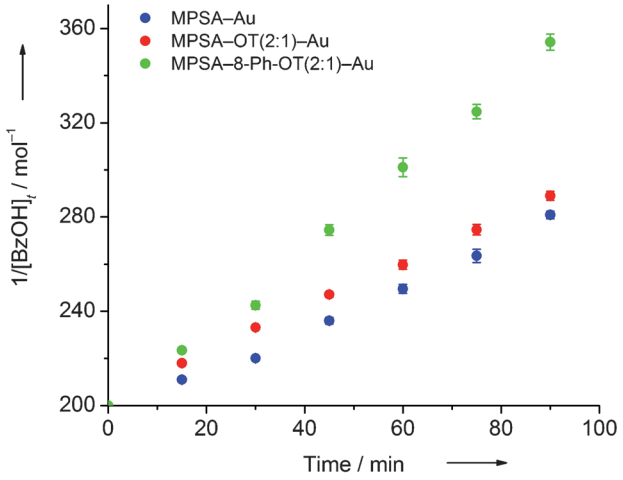

Figure 4. Plot of the reaction rate versus time for MPSA–Au, MPSA–OT(2:1)–Au and MPSA–8-Ph-OT(2:1)–Au nanoparticles as catalysts (reaction conditions: the ratio of benzyl alcohol to acetic acid was 1:1; 2 wt% catalyst; temperature 80 °C).

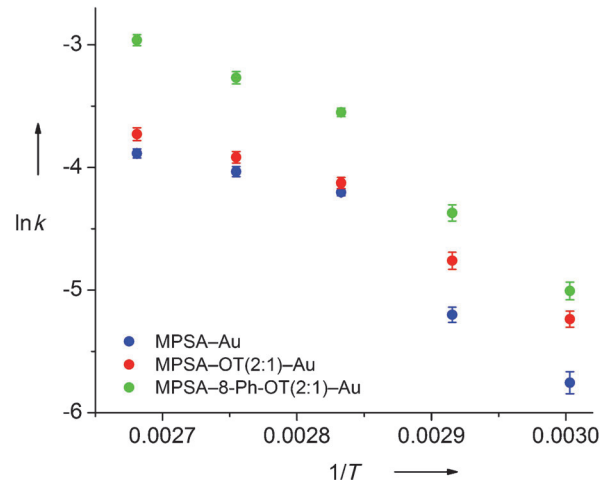

Figure 6. Arrhenius plot for MPSA–Au, MPSA–OT(2:1)–Au and MPSA–8-Ph-OT(2:1)–Au nanoparticles as catalysts.

critical temperature is reached (higher than 70 °C in the present case), there is an enhanced diffusion of the reactants into the ligand shell of the particles. This diffusion factor contributes to the temperature dependence of the pre-exponential factor of the Arrhenius equation. The energy of activation at these two different temperature regimes is summarized for the three catalysts in Table 2.

Table 2: Energy of activation for the catalytic Au nanoparticles.

Catalyst	E_{a1}[a] [kJ mol^{-1}]	E_{a2}[b] [kJ mol^{-1}]
MPSA–8-Ph-OT(2:1)–Au	71	31
MPSA–OT(2:1)–Au	54	22
MPSA–Au	76	17

[a] At temperatures of 60–80 °C. [b] At temperatures of 80–100 °C.

In conclusion, the acetylation reaction of benzyl alcohol with acetic acid has been performed in the prescence of nanoparticle catalysts functionalized with a mixture of MPSA and alkanethiols. The activity was compared with that of a conventional solid-acid zeolite USY catalyst. Formation of benzyl acetate was observed for the nanoparticle catalysts with a selectivity higher than 99%, whereas dibenzyl ether was formed as a minor product with a selectivity of around 20% by using the zeolite catalyst USY. We find that the homoligand MPSA NPs already outperform the commercial zeolite catalyst. Additionally, when we study the effect of dilution of the MPSA with OT we find the highest activity for a composition of 2:1. This finding excludes cooperative effects and indicates the role of the morphology of the ligand shell.[15] This work establishes sulfonic-acid-coated Au NPs as a new generation of solid-acid catalysts and provides the basis for studying the mixed-ligand effect of these catalysts.

Experimental Section

Materials: Chloro(triphenylphosphine)gold(I) ($AuPPh_3Cl$), borane-*tert*-butylamine complex ($tBuNH_2.BH_3$), 3-mercapto-1-propanesulfonic acid sodium salt (MPSA), 1-butanethiol (BT), 1-hexanethiol (HT), 1-octanethiol (OT), 1-decanethiol (DT), 1-dodecanethiol (DDT), 1,6-dibromohexane, 1,8-dibromooctane, 1,10-dibromodecane, phenyl lithium (PhLi), hexamethyldisilathane (HMDT), tetrabutylammonium fluoride (TBAF), benzyl alcohol (BzOH), *N*,*N*-dimethylformamide (DMF), dichloromethane (DCM), tetrahydrofuran (THF), and ethanol (EtOH) were purchased from Sigma–Aldrich. Concentrated H_2SO_4 and $MgSO_4$ were purchased from EMD Chemicals, acetic acid (AcOH), ethylacetate, hexane, and NH_4Cl were purchased from Mallinckrodt Chemicals. All chemicals were reagent grade and were used as received. The protonated form of ultrastable Y (USY) zeolite (surface area 780 $m^2 g^{-1}$) was obtained from Zeolyst International. The zeolite was activated at 150 °C before use.

Synthesis of phenyl-terminated alkanethiol ligands: In a first step bromophenyl alkanes are synthesized from the respective dibromo alkane precursor molecules. In a 100 mL round-bottomed flask equipped with a dropping funnel, 1.9 mL of a 1.14 M solution of PhLi (2.2 mmol) in hexane/diethylether was placed under N_2 atmosphere. The flask was cooled to −14 °C using a freezing mixture, and 14.5 mmol of the respective dibromo alkane in 10 mL of dry THF was added to the solution at once under stirring. The solution was allowed to stir for 6 h at −14 °C, and was then stirred at room temperature for 1 h. The reaction was quenched by dropwise addition of 20 mL of water, and the solution was then extracted with DCM. The organic layer was dried over anhydrous $MgSO_4$, and DCM was removed under vacuum at room temperature. The light yellow-colored oil was dissolved in a minimum volume of DCM, purified by chromatography on a silica column, and eluted with hexane. The solvents were removed under vacuum to yield light yellow-colored oils: 1-bromo-6-phenylhexane 2.447 g (70%), 1-bromo-8-phenyloctane 2.913 g (75%), and 1-bromo-10-phenyldecane 3.112 g (72%). ^{1}H NMR ($CDCl_3$): $\delta = 1.3$ (q, $-CH_2-$), 1.6 (q, $-CH_2-$), 1.8 (q, $-CH_2-$), 2.6 (m, $-CH_2-$), 3.5 (t, $-CH_2Br$), 7.3 (d, aromatic), 7.4 ppm (d, aromatic).

In a second step phenyl alkane thiols are synthesized from the respective bromophenyl alkanes. In a 100 mL round-bottomed flask equipped with a dropping funnel, 6.9 mmol of the respective bromophenyl alkane in 14 mL of dry THF was placed. The flask was shielded from light (to avoid photoinduced side reactions), and cooled to −20 °C using dry ice and acetone. Then a solution of 1.48 g of HMDT (8.3 mmol) and 1.98 g of TBAF (7.6 mmol) in 10 mL of THF was added to the stirred solution. The resulting mixture was allowed to warm to room temperature and stirring was continued for 12 h. After the disappearance of the bromide (monitored by TLC), the reaction mixture was concentrated to remove THF, diluted with DCM, and washed with a saturated aqueous solution of NH_4Cl. The organic layer was dried over anhydrous $MgSO_4$, and the solvent was removed under vacuum, yielding light yellow oil. The oil was dissolved in a minimum volume of DCM, purified with a neutral alumina column, and eluted with ethylacetate. The solvents were removed under vacuum to yield colorless oils: 6-phenyl-hexanethiol 1.225 g (91%), 8-phenyl-octanethiol 1.379 g (89%), and 10-phenyl-decanethiol 1.401 g (81%). ^{1}H NMR ($CDCl_3$): $\delta = 1.3$–1.4 (q, $-CH_2-$), 1.5 (t, −SH), 1.6 (q, $-CH_2-$), 2.5–2.7 (m, $-CH_2-$), 7.3 (d, aromatic), 7.4 ppm (d, aromatic).

To detect the presence of −SH groups in the synthesized thiol ligands, a solution of NaOH infused ethanol and sodium nitroprusside was added to the solution of the ligand. The resulting color change to purple indicated the presence of thiol groups.

Synthesis of composite nanoparticles: In a typical synthesis, 0.496 g of $AuPPh_3Cl$ (1 mmol) was dissolved in 50 mL of DMF. Then to a solution of requisite amounts of MPSA the alkane thiol ligand (Table 1) in 50 mL of DMF was added under stirring. The mixture was allowed to equilibriate for 10 min at 50 °C. To the mixture a solution of 0.87 g of the *tert*-$BuNH_2{\cdot}BH_3$ complex (10 mmol) in 60 mL of DMF was added dropwise. The stirring was continued at 50 °C for 1 h. After the reaction mixture was cooled to room temperature, it was kept in a freezer to precipitate the NPs overnight. The NPs were centrifuged at 3400 rpm for 5 min and washed with ethanol twice and dried under vacuum.

The terminal SO_3^- head groups were acidified by treating 100 mg of the NPs with 5 mL of 1 M H_2SO_4 for 4 h at room temperature. In the absence of this step no catalytic reaction was observed. Then 10 mL of ethanol was added to it, and kept in the freezer to precipitate the NPs overnight. The NPs were centrifuged at 3400 rpm for 5 min and washed with ethanol twice and dried under vacuum.

Catalytic testing of the composite nanoparticles: The acetylation reaction was carried out in a 25 mL two-neck round-bottomed flask fitted with a reflux condenser and containing a tiny magnetic stir bar. In a typical experiment, 0.54 g of benzyl alcohol (5 mmol), 0.3 g of acetic acid (5 mmol), and 10 mg of the nanoparticle catalyst were taken directly into the reaction vessel (for the relative amount of active sites refer to Table 1) and sonicated for 2 min to disperse the nanoparticles uniformly in the reaction medium. The reaction vessel was immersed in an oil bath and put on a IKAMAG RCT basic hot plate with a magnetic stirrer. The temperature of the oil bath was controlled by an IKA ETS-D5 electronic contact thermometer connected to the hot plate. The reaction mixture was stirred at 80 °C and at 600 rpm for 6 h. For the experiments with the zeolite USY catalyst, 75 mg of the catalyst was used.

However, experiments were also performed by varying the reaction temperature (60–100 °C), and the reaction time (0–6 h) to obtain various kinetic parameters. The reaction mixture was continuously stirred during the reaction at a constant temperature. After the desired reaction time, the catalyst was separated from the reaction mixture by centrifugation at 14000 rpm for 5 min and washed with ethanol.

For the kinetic experiments, 25 μL of the reaction mixtures was sampled every 15 min and the samples were kept in a freezer overnight to precipitate the NPs. After centrifugation, the reaction mixtures were diluted with 1 mL ethanol and analyzed by gas chromatography (GC). The main product of the reaction was found to be benzyl acetate. The formation of dibenzyl ether was also observed when USY was used as catalyst.

Analytic measurements: TEM experiments were carried out on a JEOL 200CX instrument operated at 200 kV. The core sizes of the NPs were determined using TEM images. The diameter of around 1000 NPs per sample was estimated and averaged using ImageJ software.

XPS experiments were performed on a Kratos Axis Ultra X-ray photoelectron spectrometer employing a monochromatic Al K_α source (1486.7 eV) and an electron takeoff angle of 90° relative to the sample plane. The survey scan was conducted at a pass energy of 80 eV for binding energies (BEs) ranging from 0–1100 eV. The high-resolution scans of O 1s, C 1s, S 2p, and Au 4f were conducted at a pass energy of 10 eV. The core-level spectra were corrected for the background using the Shirley algorithm and the core-level BE was aligned with respect to the Au $4f_{7/2}$ BE of 84 eV.

The reaction products were analyzed by a gas chromatograph from Agilent containing a polyethylene glycol capillary column and a flame ionization detector (FID).

Received: March 14, 2011
Revised: May 31, 2011
Published online: July 8, 2011

Keywords: catalysts · gold · heterogeneous catalysis · nanoparticles

[1] M. C. Daniel, D. Astruc, *Chem. Rev.* **2004**, *104*, 293.
[2] A. P. Alivisatos, *Science* **1996**, *271*, 933.
[3] M. Bartz, J. Kuether, R. Seshadri, W. Tremel, *Angew. Chem.* **1998**, *110*, 2646; *Angew. Chem. Int. Ed.* **1998**, *37*, 2466.
[4] C. Briggs, T. B. Norsten, V. M. Rotello, *Chem. Commun.* **2002**, 1890.
[5] L. Pasquato, P. Pengo, P. Scrimin, *Supramol. Chem.* **2005**, *17*, 163.
[6] F. Manea, F. B. Houillon, L. Pasquato, P. Scrimin, *Angew. Chem.* **2004**, *116*, 6291; *Angew. Chem. Int. Ed.* **2004**, *43*, 6165.
[7] A. M. Jackson, J. W. Myerson, F. Stellacci, *Nat. Mater.* **2004**, *3*, 330.
[8] A. M. Jackson, P. Jacob Silva, Y. Hu, F. Stellacci, *J. Am. Chem. Soc.* **2006**, *128*, 11135.
[9] G. A. DeVries, M. Brunnbauer, Y. Hu, A. M. Jackson, B. Long, B. T. Neltner, O. Uzun, B. H. Wunsch, F. Stellacci, *Science* **2007**, *315*, 358.
[10] A. Centrone, Y. Hu, A. M. Jackson, G. Zerbi, F. Stellacci, *Small* **2007**, *3*, 814.
[11] C. Singh, P. K. Ghorai, M. A. Horsch, A. M. Jackson, R. G. Larson, F. Stellacci, S. C. Glotzer, *Phys. Rev. Lett.* **2007**, *99*, 226106.
[12] C. Singh, A. M. Jackson, F. Stellacci, S. C. Glotzer, *J. Am. Chem. Soc.* **2009**, *131*, 16377.
[13] A. Centrone, E. Penzo, M. Sharma, J. W. Myerson, A. M. Jackson, N. Marzari, F. Stellacci, *Proc. Natl. Acad. Sci. USA* **2008**, *105*, 9886.
[14] J. J. Kuna, K. Voitchovsky, C. Singh, H. Jiang, S. Mwenifumbo, P. K. Ghorai, M. M. Stevens, S. C. Glotzer, F. Stellacci, *Nat. Mater.* **2009**, *8*, 837.
[15] O. Uzun, Y. Hu, A. Verma, S. Chen, A. Centrone, F. Stellacci, *Chem. Commun.* **2008**, 196.
[16] R. P. Carney, G. A. DeVries, C. Dubois, H. Kim, J. Y. Kim, C. Singh, P. K. Ghorai, J. B. Tracy, R. L. Stiles, R. W. Murray, S. C. Glotzer, F. Stellacci, *J. Am. Chem. Soc.* **2008**, *130*, 798.
[17] N. Zheng, J. Fan, G. D. Stucky, *J. Am. Chem. Soc.* **2006**, *128*, 6550.
[18] W. T. Liu, C. S. Tan, *Ind. Eng. Chem. Res.* **2001**, *40*, 3281.
[19] A. Zaidi, J. L. Gainer, G. Carta, *Biotechnol. Bioeng.* **1995**, *48*, 601.
[20] S. R. Kirumakki, N. Nagaraju, S. Narayanan, *Appl. Catal. A* **2004**, *273*, 1.
[21] G. Zaupa, C. Mora, R. Bonomi, L. J. Prins, P. Scrimin, *Chem. Eur. J.* **2011**, *17*, 4879.
[22] S. Kato, K. Nakagawa, N. Ikenaga, T. Suzuki, *Catal. Lett.* **2001**, *73*, 175.